Controlled-synthesis of Hierarchical $NiCo_2O_4$ anchored on carbon nanofibers mat for Free-Standing and Highly-Performance supercapacitors

M Hussein El-Shafei[1,2], Ahmed G. El-Deen[3], Ahmed Abd El-Moneim[2,4], Amr Hessein[2,5]

[1]Production engineering and mechanical design department, Mansoura University, El-Mansoura 35516, Egypt.

[2]Graphene Center of Excellence for Energy and electronic Applications, Egypt-Japan University of Science and Technology, Alexandria 21934, Egypt.

[3]Renewable Energy Science and Engineering Department, Faculty of Postgraduate Studies for Advanced Sciences (PSAS), Beni- Suef University, Beni-Suef 62511, Egypt

[4]Institute of Basic and Applied Sciences, Egypt-Japan University of Science and Technology, New Borg El Arab, Alexandria 21934, Egypt.

[5]Department of Mathematical and Physical Engineering, Faculty of Engineering (Shoubra), Benha University, Cairo 11614, Egypt.

Abstract

In this work, a versatile one-step hydrothermal technique was used to produce a hybrid standalone electrode of $NiCo_2O_4$ hierarchical nanostructures anchored on CNFs mat for highly-performance and substrate-free supercapacitors. The CNFs mat was working as a conductive and a three-dimensional template for hierarchical $NiCo_2O_4$ nanostructures deposition at the same time. The morphological and structural data analysis revealed a pure spinel $NiCo_2O_4$ nanostructures with a unique surface morphology comprising interconnected ultrathin nanoneedles and nanoflowers were successfully anchored to the CNFs mat. Real supercapacitors consist of two-symmetrical hybrid electrodes with

different $NiCo_2O_4$ loading ratios were assembled and tested. The electrochemical performances of the assembled devices in terms of specific capacitance, energy, and power densities were systematically evaluated. Increasing the $NiCo_2O_4$ loading on the CNFs mat had shown a positive impact on improving the overall electrochemical performance of the assembled supercapacitors. A hybrid electrode loaded with $NiCo_2O_4$ twice as much as CNFs possess a specific capacitance value of 540 F g^{-1} along with an energy density of 30 Wh kg^{-1} at a power density of 515.6 W kg^{-1}. In addition, the device showed excellent cycling stability and high capacitance retention against 6000 charge-discharge cycles at a charging current of 1.0 A g^{-1}.

Keywords: $NiCo_2O_4$; CNFs; hybrid nanocomposite; electrochemical capacitance; free-standing supercapacitors

1. Introduction

The upcoming times will witness more spreading of flexible and wearable electronics for various oriented applications such as medical treatment purposes, smart assistance devices, and also the remote sensing devices **[1,2]**. This would indeed be accompanied by increasing the demands on highly-performance and flexible energy storage devices to meet the electric energy requirements of such applications. Nevertheless, lightweight, environmentally safe, long cyclic life in addition to fast recharge capability are prerequisites for these types of power sources **[3]**. A supercapacitor (SC) is an electrochemical storage device that combines the merits of the high-power from the traditional dielectric capacitors and the high-energy-density from conventional batteries together in one device **[4]**.

Recently, the flexible SCs became more attractive as power sources than micro-batteries owing to its unique qualities of flexibility and high rate capabilities **[5]**. Flexible SC devices built from various electrode materials have been already fabricated and tested. Many carbon nanostructures in the form of stand-alone and on flexible substrates such as carbon nanotubes (CNTs) **[6,7],** graphene **[8,9]**, mesoporous carbon **[10]**, and carbon nanofibers (CNFs) **[11]** have been explored for a long time. Although carbon allotropes are chemically stable and non-toxic materials, however, and due to its intrinsic electric double layer (EDL) storing mechanism the devices are usually suffered from low specific capacitances (commonly lower than 400 F g^{-1}) and poor power density **[12–14].**

Alternatively, SC electrodes from materials Relies on the pseudocapacitance storing mechanism had been proven to attain much higher specific capacitances and power densities than EDL carbonaceous materials **[15]**. Among a large number of the fabricated and tested pseudocapacitive materials, flexible SCs based on metal oxides electrodes such as RuO_2 **[16]**, MnO_2 **[17–19]** , NiO **[20]**, and Co_3O_4 nanostructures **[21,22]** were got attention due to their outstanding performances and not to contain toxic elements such as sulfides and selenides. Although the promising performance of RuO_2 Flexible SC (as high as 700 F g^{-1}), its large-scale application is restricted by its rareness in nature [23–26]. On the other side, the large-scale applications of earth-abundant metal oxides (MnO_2, NiO, Co_3O_4, …etc) in flexible SC devices are hindered by their inferior electric conductivity, low specific capacitances than RuO_2 besides the relatively short cycling life compared to carbon-based devices [27,28]. Hence, there was an exigent necessity for developing robust and scalable approaches to fabricate hybrid electrodes for flexible SCs bridging the

preferable qualities of abundance, chemical stability, and also excellent electrochemical storage performance from both metal oxides and carbon nanostructures.

As a newly leading material, nickel cobaltite ($NiCo_2O_4$) has got considerable attention as a pseudocapacitive electrode material because it possesses better electrochemical activity and electrical conductivity at least two orders of magnitude higher than pure Co_3O_4 and NiO [12,29]. Despite the promising results the $NiCo_2O_4$-based SCs were achieved, the reported studies considering $NiCo_2O_4$ nanostructures in real two-electrode flexible SC devices still very rare. For instance, Jun Du et al. electrodeposited ultrathin porous $NiCo_2O_4$ nanosheets on a flexible carbon fabric and recorded a 2658 F g^{-1} specific capacitance using a three-electrode system [30]. Also, F. Deng and his coworkers reported in 2015 the solvothermal synthesis of mesoporous $NiCo_2O_4$ nanosheets on carbon fiber paper and they achieved as high as 1036 F g^{-1} specific capacitance, but it was also using a three-electrode system [29,31].

In this regard, this study introduces a scalable and readily approach for the fabrication of highly-performance, free-Standing, and flexible SC real devices based on hybrid nanocomposites from a CNFs mat decorated by $NiCo_2O_4$ nanostructures. Herein, the conductive CNFs mats are served as a free-standing flexible electrode as well as the porous framework for the deposition of the $NiCo_2O_4$ nanostructures. The CNFs mats were firstly obtained by the high-temperature carbonization of electrospun polyacrylonitrile nanofiber mats. $NiCo_2O_4$ nanostructures with different loading mass ratios were grown onto the CNFs electrode using the facile hydrothermal method. The free-standing SCs based on $NiCo_2O_4$:CNFs hybrid electrodes attained remarkable electrochemical performances those far exceeding the devices from bare CNFs, NiO:CNFs, and also Co_3O_4:CNFs electrodes.

The electrochemical measurements performed on real two-electrode SC fabricated based on the flexible $NiCo_2O_4$:CNFs hybrid nanocomposite showed a very high specific capacitance that reached 540 F g^{-1} and also a maximum energy density of 30 Wh kg^{-1} at a remarkable power density of 515.6 W kg^{-1} as well as excellent cycling stability. The performances of the hybrid nanocomposites were carefully interpreted and evaluated from the structural and morphological characterization employed in this study.

2. Experimental work

2.1 Materials

All precursors for CNFs and metal oxides preparations such as polyacrylonitrile (PAN, Mw≈150000 $g.mol^{-1}$), Cobalt(II) nitrate $Co(NO_3)_2$ 98%, Nickel(II) nitrate $Ni(NO_3)_2$, and urea [$CO(NH_2)_2$, >99%] were purchased from Sigma–Aldrich and used as received. N, N-dimethy1formamide (DMF) was purchased from Fisher Scientific, and ethanol was obtained from Sigma–Aldrich as a reagent grad, and both solvents were used without additional purifications.

2.2 Preparation of free-standing CNFs mat.

The freestanding CNFs mat was prepared according to our previous procedure [32]. In a typical procedure, a PAN nanofibers mat was first prepared to form a polymeric solution of 8 wt. % PAN in DMF using an electrospinner (Nanon-01 electrospinner, MECC, Japan). The electrospinning process was performed at a constant feed rate of 1.5 ml h^{-1} and an applied voltage of 25 kV. The distance between the spinneret and the collecting drum was kept fixed at 15 cm, while the drum speed was constant at 500 RPM.

At the end of the electrospinning process, the PAN nanofibers mats were collected and dried at 50 ºC for at least 12 hours under vacuum.

In order to obtain the conductive CNFs mat, the carbonization process of the PAN nanofibers mat was carried out at two stages. Firstly, is the oxidative stabilization stage in which the PAN mat was annealed in air at 280 ºC for 3 hours at a heating rate of 1.0 ºC min^{-1}. Secondly, is the carbonizing stage in which the stabilized PAN mat was annealed under argon flow at 1100 ºC for one hour with a heating rate of 4.0 ºC min^{-1} in a tubular furnace. The renewed argon flow was used to prevent the oxidation as well as eliminate the impurities and byproducts such as N_2, CO_2, and H_2O. The free-standing CNFs mat preparation procedure is schematically summarized in Fig. 1**.**

2.3 Synthesis of $NiCo_2O_4$ nanoparticles coated carbon nanofiber

The synthesis of $NiCo_2O_4$ nanostructures anchored on CNFs mat with different loadings ($NiCo_2O_4$@CNFs) ratio were synthesized using a simple hydrothermal method [33]. The reaction vessel is a 100 ml Teflon-lined stainless-steel autoclave reactor containing 75 ml of the reactant solution and the CNFs mat. Firstly, the reactant solution was prepared separately by dissolving the proper amounts of $Co(NO_3)_2$ and $Ni(NO_3)_2$ in a doubled distilled water by a magnetic stirrer. After the complete dissolving, a 9.0 mmol of urea granules were added and stirred for 0.5 hour and then transferred to the Teflon cup of the reactor. After that, a square pieces of neat CNFs has a mass of 50 mg was soaked into the obtained solution and for 1 hour. The autoclave reactor is then sealed and maintained at 160 ºC for 16 hours. After cooling down to room temperature, the CNFs mat coated with Ni-Co precursor was extracted then washed with DI water and ethanol several times to remove unreacted slats and dried overnight in a vacuum oven at 60 ºC. The dried samples

are finally calcinated at 360 ºC in air for 2 hours with a heating rate of 3 ºC min^{-1}. Three different loadings ratios of $NiCo_2O_4$ on CNFs mat were prepared, as indicated in Table 1. The loading was calculated according to the final yield of the reactant precursor with respect to the mass of the CNFs mat. Herein, a maximum loading ratio of $NiCo_2O_4$:CNFs that can be synthesized was 2: 1 due to the capacity limitation of the CNFs mat. Higher loading of $NiCo_2O_4$ on the CNFs was could not be achieved under our experimental setup. Such that, the usage of higher initial quantities of the metal salts showed no increase in the loading of the anchored $NiCo_2O_4$ on the CNFs mat as calculated from the final yielded of $NiCo_2O_4$:CNFs to the precipitate powder. Finally, a pure ultrathin porous $NiCo_2O_4$ nanostructures were fabricated using the same procedure, but in the absence of CNFs mat.

Table 1: Summary of initial components used for fabricating $NiCo_2O_4$:CNFs with different loading ratios.

Sample name	$NiCo_2O_4$:CNFs ratio	CNFs (mg)	$Co(NO_3)_2$ (mmol)	$Ni(NO_3)_2$ (mmol)
$NiCo_2O_4$ 1:2 CNFs	1:2	50	1.0	0.5
$NiCo_2O_4$ 1:1 CNFs	1:1	50	2.0	1.0
$NiCo_2O_4$ 2:1 CNFs	2:1	50	4.0	2.0
$NiCo_2O_4$	--	0	1.0	0.5

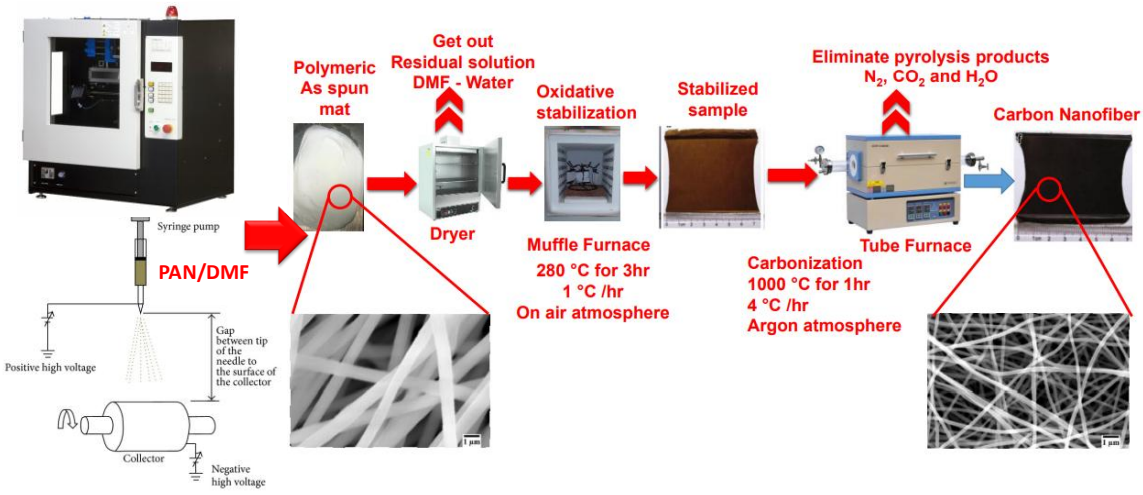

Fig. 1: The workflow of the standalone CNFs mat preparation steps.

2.4 Materials characterization:

The surface morpho1ogy of the carbon nanofibers was investigated using a scanning e1ectron microscope technique (SEM) (JEOL JSM-6010LV (Tokyo, Japan). A high-reso1ution transmission e1ectron microscope (HR-TEM) (JEOL JEM- 2010F) was also used for further morphology characterization. The structure of carbonized fibers was investigated by X-Ray Diffractometer (XRD) (Shimadzu Xlab 6100, Japan) using Cu Kα radiation. Fourier Transform Infrared (FT-IR) spectrometer (Bruker Vertex 70, Germany) was used for the analysis of the chemical composition of the fibers. Raman spectra of the carbonized nanofibers were examined using a Thermo Fisher Scientific Inc., MA, USA.

2.5 Electrochemical measurements

The electrochemical performance of the supercapacitor (SC) device based on hybrid $NiCo_2O_4$:CNFs nanocomposites electrode was examined in the form of symmetric two electrodes system using cyc1ic vo1tammetry (CV), galvanic charge-discharge (GCD), and electrochemical impedance spectroscopy (EIS) tests. Two pieces 2 cm × 2 cm from the hybrid $NiCo_2O_4$:CNFs electrode were assembled using a spacer and 1 M KOH solution as the electrolyte. The standalone $NiCo_2O_4$:CNFs mats were used here as the supercapacitor electrode as well as the current collector, whereas the electric connections were made from a bare terminal without deposited $NiCo_2O_4$. All e1ectrochemical measurements were performed using potentiostat/galvanostat (PARSTAT 4000+ workstation).

The specific capacitance (C_s) was ca1cu1ated from the GCD measurement in accordance with **Eq (1)**.

$$C_{s=}\frac{I\times\Delta t}{M\times\Delta V} \qquad (1)$$

Where I is the discharge current (0.25 - 7.0 mA), ΔV is the voltage window in volts during the discharging process, Δt is the discharge time in seconds. The power density (*P)* and energy density (E) of the fabricated devices were calculated using **Eq (2) and (3)**:

$$E = \frac{1}{2} \times C_s \times (\Delta V)^2 \qquad (2)$$

$$P = \frac{E}{\Delta t} \qquad (3)$$

3. Results and discussion

3.1 Structural characteristics of the $NiCo_2O_4$:CNFs hybrid nanocomposites

The hydrothermal approach proposed here is a one-step technique intended for the formation of highly-performance standalone hybrid $NiCo_2O_4$:CNFs electrodes for flexible supercapacitor applications. **Fig. 2** is a schematic representation that suggests the $NiCo_2O_4$ nanostructures formation mechanism on the CNFs mat. Simply, the dissociation of the metal nitrates in water releases plenty of Ni^{2+} and Co^{2+} metallic cations. When the CNFs mats were soaked into this solution, Ni^{2+} and Co^{2+} were electrostatically attached to its surface and also within the CNFs network by the action of the sonication power. During the hydrothermal process and as the temperature of the reacting bath is increasing, the urea granules were slowly decomposing and produce a large number of OH^- ions:

$$CO(NH_2)_2 + nH_2O \rightarrow nNH_4OH + CO_2 \uparrow$$

$$nNH_4OH + CsH_4{}^+ + nOH^-$$

The OH^- ions start to react with the metallic Ni^{2+} and Co^{2+} ions initiating the nucleation and the growth of mixed double hydroxides $[(Ni,Co)(OH)_6]$ on the surface of the CNFs mats. Increase the reaction temperature up to 160 ºC and increasing the concentration of

the reactants are two factors responsible for the increment of the deposited mixed double hydroxides on the surfaces of the CNFs mats:

$$(Ni^{2+}, 2Co^{2+}) + nOH^{-} \rightarrow (Ni, Co)(OH)_6 + \frac{1}{2}O_2$$

The hydrothermally grown of (Ni, Co)$(OH)_6$ onto CNFs substrates were converted to $NiCo_2O_4$:CNFs electrodes by the calcination process that performed at 360 ºC in the presence of the oxygen environment which also helped in releasing the bonded water molecules out of the electrodes:

$$(Ni, Co)(OH)_6 + \frac{1}{2}O_2 \rightarrow NiCo_2O_4 + 3H_2O$$

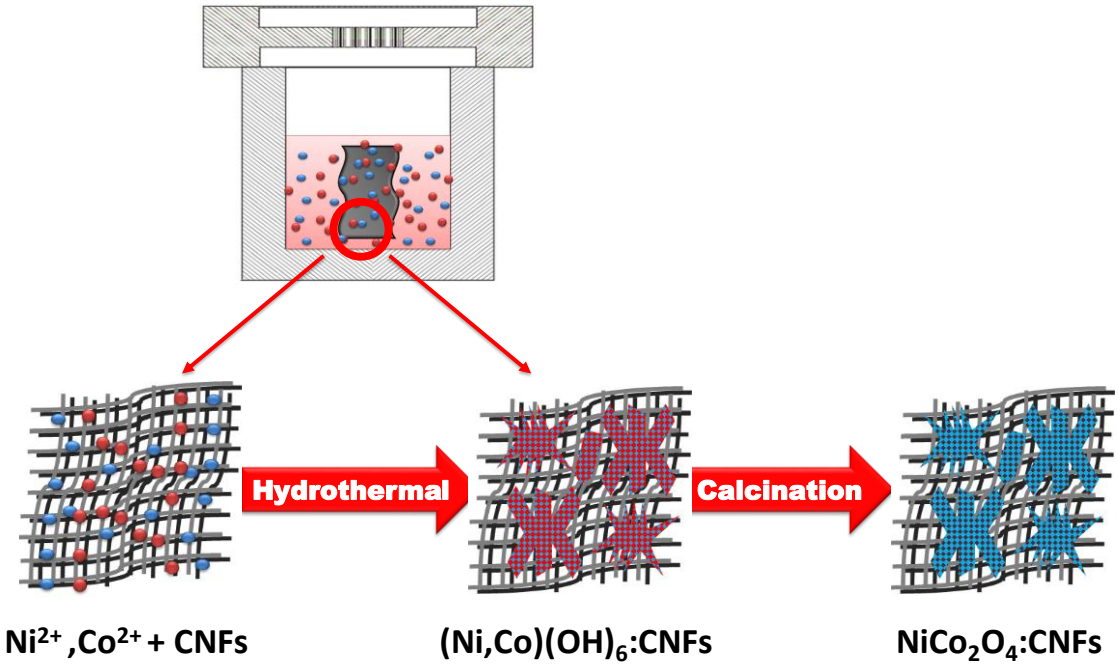

Fig. 2: Schematic representation of the suggested formation mechanism of the $NiCo_2O_4$ nanostructures on the CNFs mat.

The XRD patterns collected from the prepared materials presented in **Fig. 3**(a) show the diffraction peaks related to the $NiCo_2O_4$ are superimposed on the XRD diffraction pattern of the neat CNF, indicating the successful synthesis of the $NiCo_2O_4$:CNFs hybrid nanocomposite. The diffraction peaks of (220), (311), (400), (511) and (440) reflection

planes located at 2θ values of 31.2º, 36.7º, 44.6º, 59.1º, and 65º respectively, are assigned to the cubic spinel $NiCo_2O_4$ phase (JCPDS card No. 20-0781), with no other peaks belong to single oxide phases. However, the diffuse nature appeared as broadening in the $NiCo_2O_4$ peaks in the nanocomposite pattern compared to those of the pristine $NiCo_2O_4$ confirming the nanostructure nature of the deposited oxides.

Further confirmations on the phase purity of the $NiCo_2O_4$ nanostructured and the attachment quality on the CNFs mat were conducted by Raman scattering and FTIR spectroscopic measurements as depicted in **Fig. 3(b)** and **Fig. 3(c)** respectively. The single peak appeared at 658 cm^{-1} wavenumber besides the D and G peaks of the CNFs in the Raman spectrum of $NiCo_2O_4$ 2:1 CNFs nanocomposite, **Fig. 3**(b), was assigned to the A_{1g} vibrational active mode of the $NiCo_2O_4$ spinel oxide [34]**.** Also, the noticeable increase in the intensity of the G-band with respect to the D-band after loading with $NiCo_2O_4$ is observed, such that the (I_D/I_G) ratio was decreased from 0.97 in the case of neat CNFs mat to be 0.78 in the case of the $NiCo_2O_4$ 2:1 CNFs nanocomposites. This is firmly attributed to the enhancements in the graphitization degree of the CNFs by the action of hydrothermal and the calcination treatments [35]. Along the same lines, the FTIR spectra of both the neat CNFs mat and the $NiCo_2O_4$:CNFs nanocomposites in **Fig. 3(c)** showed the same FTIR bands as indicated except that, the spectrum for $NiCo_2O_4$ 2:1 CNFs composite revealed the presence of two strong bands at lower frequencies of 557 and 652 cm^{-1}. Those observed new peaks were firmly assigned to the stretching vibrations of the Ni-O and Co-O bonds in the nickel-cobalt oxide, respectively [36]. These results confirm to a large extent on the formation of a well-anchored and pure spinel $NiCo_2O_4$ nanostructures on the CNFs mat.

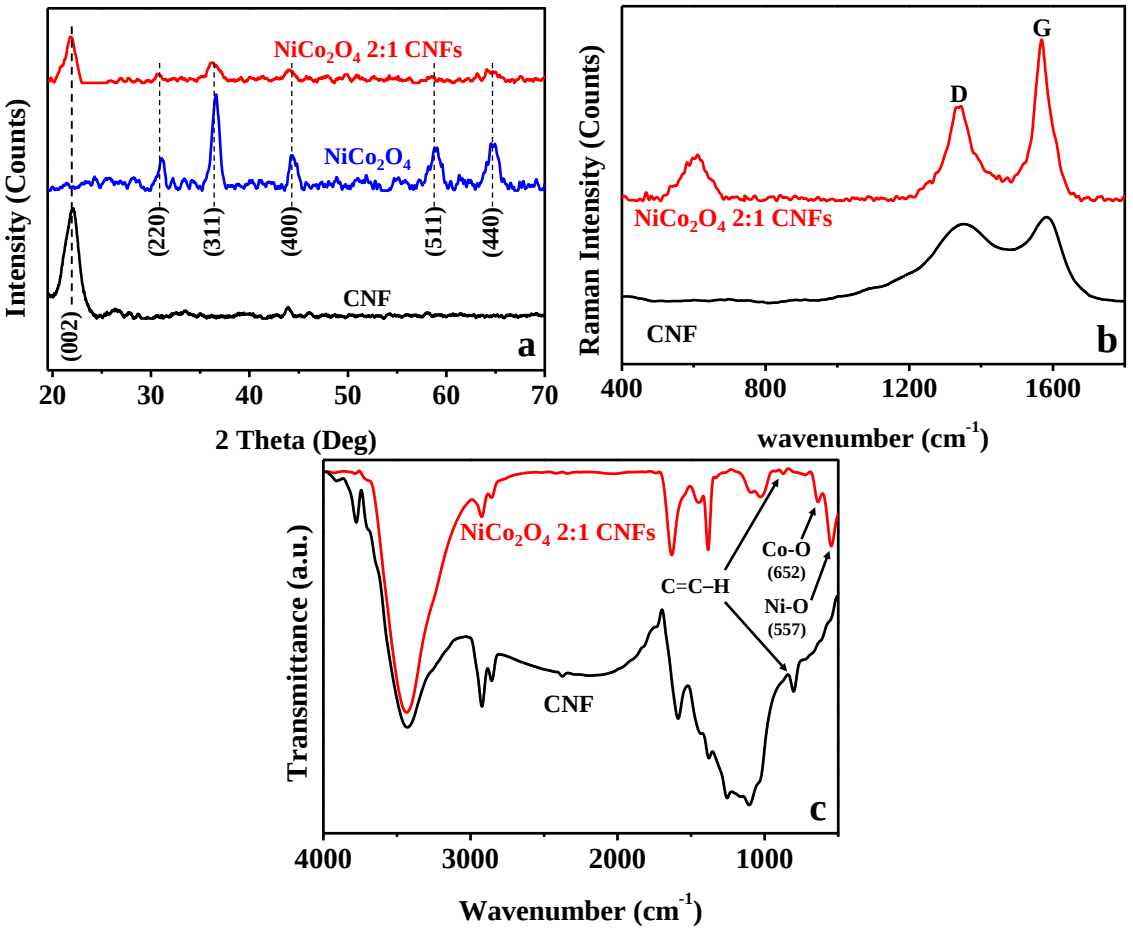

Fig. 3: (a) XRD patterns, (b) Raman spectra and (c) FTIR, for neat CNFs and $NiCo_2O_4$ 2:1 CNFs hybrid nanocomposite.

3.2 Morphological characteristics of the $NiCo_2O_4$:CNFs hybrid nanocomposites

The surface morphology of the neat CNFs mat and the hybrid $NiCo_2O_4$:CNFs electrodes were inspected by means of SEM and the inspection results are shown in **Fig. 4**. The low-magnification micrograph of the neat CNFs mat in **Fig. 4(a)** revealed a continuous fibers network with a smooth surface and beads free those have an average diameter of ~300 nm. Whereas the high-magnification micrograph in **Fig. 4(a1)** shows that the CNFs are fused together and formed a conductive porous network. This unique structure of the CNFs mat is not only providing a high exposed area for the deposition of the pseudoactive oxides and electrolyte infiltration but also offers plenty of conductive channels through the electrode to facilitate the swift charge carriers kinetics. Furthermore, the rigid CNFs conductive

network affords a robust mechanical template that satisfies the flexibility and conductivity necessity requirements for a standalone supercapacitor electrode.

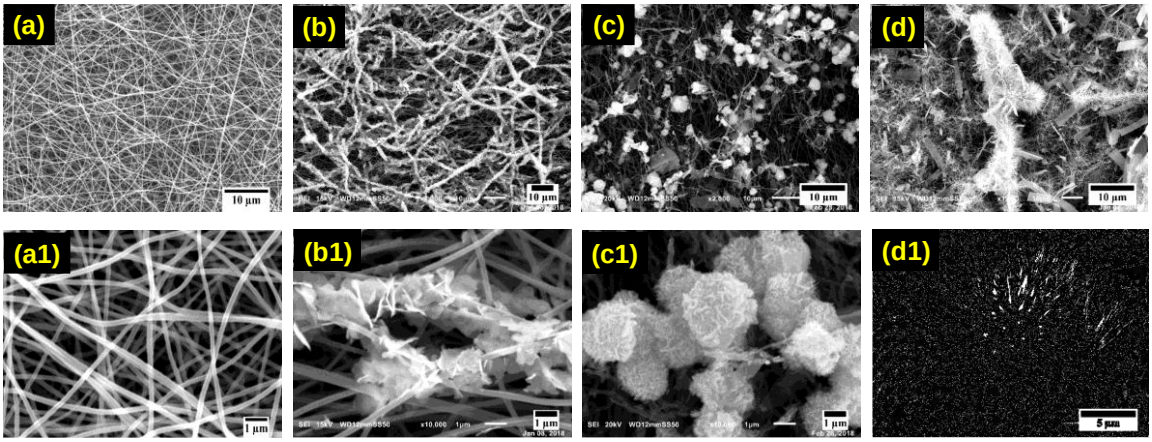

Fig. 4: SEM micrographs for (a, a1) neat CNFs, (b,b1) $NiCo_2O_4$ 1:2 CNFs, (c,c1) $NiCo_2O_4$ 1:1 CNFs, (d,d1) $NiCo_2O_4$ 2:1 CNFs.

The SEM micrographs of the $NiCo_2O_4$:CNFs hybrid nanocomposites **Fig. 4(b) – (d)** show a uniform and non-uniform coating of the CNFs mat with $NiCo_2O_4$ hierarchical nanostructures. An increase in the coating uniformity along with a change in the $NiCo_2O_4$ morphology were clearly observed with increasing the initial concentrations of the metal salt precursors in the reacting bath. The surface morphology of $NiCo_2O_4$ was changed from nanoparticles and nanoflakes morphology for the $NiCo_2O_4$ 1:2 CNFs electrode to nanoflowers morphology for the $NiCo_2O_4$ 1:1 CNFs electrode, and to hierarchical nanorods with needle-like shape for the $NiCo_2O_4$ 2:1 CNFs electrode. Such ideal porous networks of the electrodes with a high loading of the $NiCo_2O_4$ hierarchical nanostructure supported on the conductive CNFs would enable more redox reactions to occur for high charge/discharge rates as well as increasing the electrodes specific capacitances.

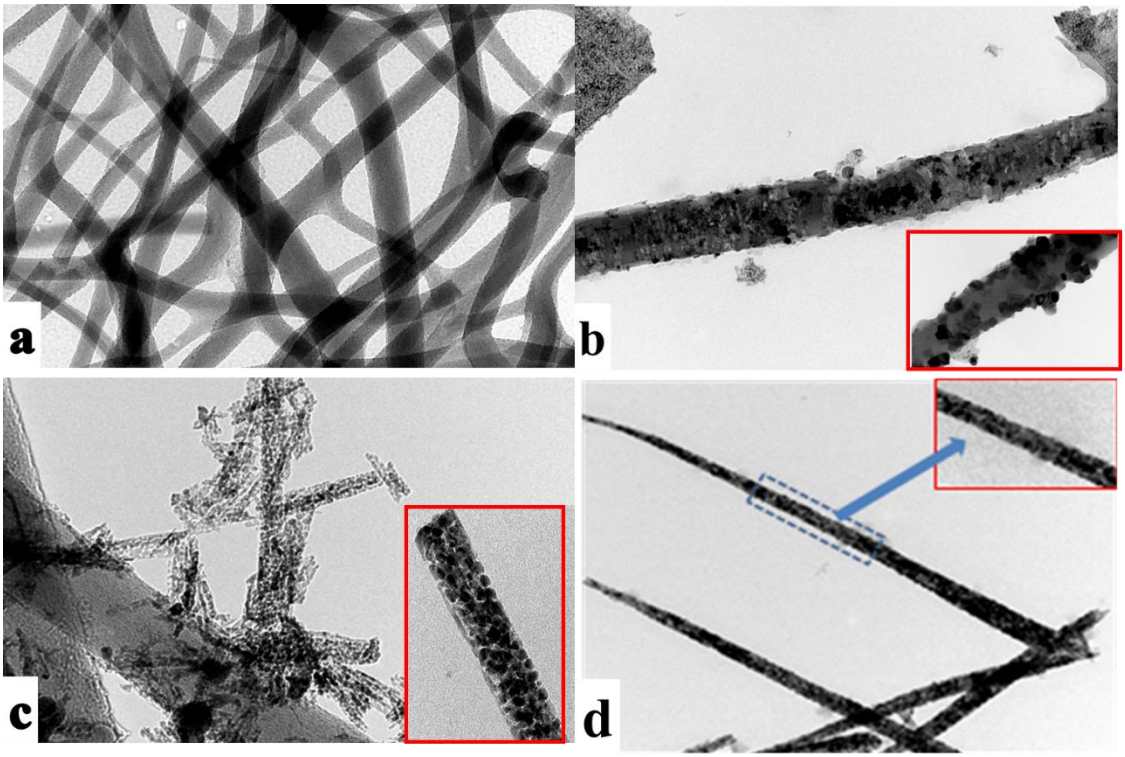

Fig. 5: TEM micrographs for (a) neat CNFs, (b,) $NiCo_2O_4$ 1:2 CNFs, (c) $NiCo_2O_4$ 1:1 CNFs, (d) $NiCo_2O_4$ 2:1 CNFs.

The acquired TEM micrographs in **Fig. 5** give a closer look at the nature of the $NiCo_2O_4$ nanostructures coated on the CNFs mat. The TEM micrograph of the neat CNFs in **Fig. 5**(a) confirm the excellent morphology of the CNFs without any beads or cracks and also shows the perfect cross-linked sites. After the $NiCo_2O_4$ hydrothermal deposition, the micrograph of the $NiCo_2O_4$ 1:2 CNFs electrode in **Fig. 5(a)** shows that the plain surface of CNFs were coated with the $NiCo_2O_4$ nanoparticles. The TEM images of the $NiCo_2O_4$ 1:1CNFs and $NiCo_2O_4$ 2:1 CNFs samples with higher loadings given in **Fig. 5 (c)** and **(d)** show the spinal $NiCo_2O_4$ nanoparticles connected together to form either hierarchical nanoflowers or nanorods, respectively. The enlarged inset views of both samples disclose the ultra-porous structure of the hierarchical $NiCo_2O_4$ nanostructures those having an average pores diameter of 2–4 nm.

In brief, an excellent electrochemical electrode composed of the $NiCo_2O_4$ nanostructures anchored on CNFs conductive as flexible hybrid electrode was directly synthesized. Based on the 3D hierarchical structure of $NiCo_2O_4$:CNFs nanocomposites synthesized with high mass loading of the pure and crystalline $NiCo_2O_4$ electrochemical catalyst, a remarkable electrochemical performance is anticipated to be achieved for many reasons. First, the CNFs mat represents an ideal 3D structure composed of highly-conductive nanofibers that served as an excellent open scaffold to load high concentrations from $NiCo_2O_4$ in the form of ultrathin nano-needles. This is suggested to facilitate the electrons and ions transport along and within the hybrid electrode. Second, the uniform distribution of $NiCo_2O_4$ nano-flower with interconnected nano-needles structure provides high exposed surface area rich with superabundant active sites ready for participating in enormous Faradic reactions. This is suggested to lead to high electrochemical capacitance and to satisfying rate capability. Lastly, the in-situ growth of $NiCo_2O_4$ nanostructure directly on the CNFs gave us the opportunity to avoid the usage of additional conductive additives or even the usage of the charge-transport-hindering polymeric binders. Thus, a high mechanical stability and an improved electrical conductivity are additional expected advantages of our prepared hybrid electrodes than other similar hybrid nanocomposites reported previously in the literature [37,38].

3.3 Electrochemical performance of the $NiCo_2O_4$:CNFs hybrid nanocomposites

The electrochemical performances of the $NiCo_2O_4$:CNFs hybrid nanocomposites as standalone flexible supercapacitors were examined by means of CV, GCD, and EIS, measurements performed on a two-symmetrical electrodes supercapacitor configuration. As shown in **Fig. 6(a)**, each device was composed of two rectangular symmetric pieces of

$NiCo_2O_4$:CNFs as a device electrodes, 1 M KOH aqueous electrolyte, and polyethylene /polypropylene (PP/ PE) separator. In the assembled devices, the CNFs mat acts as the standalone substrate and the current collectors at the same time. Worthwhile to mention that, the $NiCo_2O_4$ nanostructure was carefully removed from the edges before the assembly to ensure making a good contact between the device and the potentiostat leads. After the assembly, the devices were let for about one hour before performing the measurements to permit the electrolyte to completely diffused and wet the electrodes.

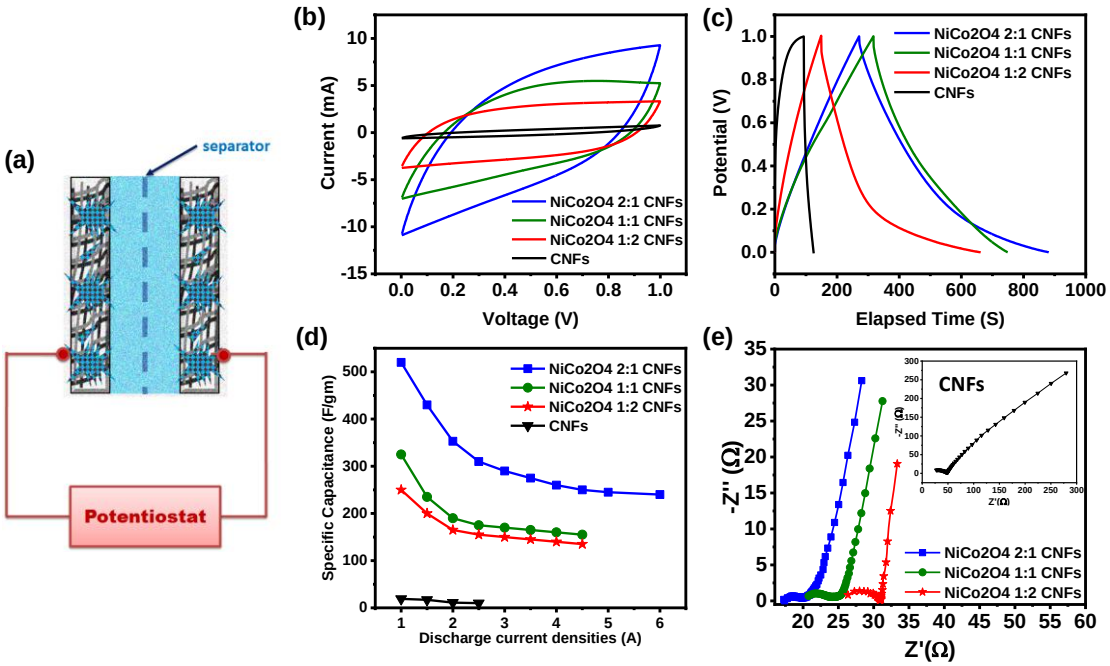

Fig. 6: (a) Schematic diagram of the device configuration comprising two-symmetric $NiCo_2O_4$:CNFs electrodes, (b) CV voltammograms at a scan rate of 50 mVs^{-1}, (c) charge-discharge curves at current density 1A g^{-1}, (d) the specific capacitances at different current densities (1-7 Ag^{-1}), and (e) EIS Nyquist curves of two-symmetric electrodes SC devices fabricated based on different $NiCo_2O_4$:CNFs loading ratios.

Fig. 6 (b) displays the CV voltammograms for all fabricated SC devices measured at 50 mV s^{-1}. Noticeably, all the CV voltammograms of the $NiCo_2O_4$:CNFs devices yielded higher current densities and attained larger enclosed area than the neat CNFs device. This

observation affirms on the effective pseudocapacitive role of the $NiCo_2O_4$ nanostructures played in enhancing the electrochemical capacitance of the devices. This was also noticed from the quasi-rectangular CV voltammograms exhibited by all the curves of the $NiCo_2O_4$:CNFs devices, unlike the rectangular voltammogram of the neat CNFs- based device. The transformation to quasi-rectangular was increased by increasing the $NiCo_2O_4$ mass loading ratio on the CNFs electrode. Furtherly, the enclosed area of these voltammograms, which qualitatively corresponds to the specific capacitance (*Cs*) of the devices, increases with increasing the loading ratio of the $NiCo_2O_4$ on the CNFs. These observations indicate the enhancements in the overall devices' capacitances with increasing the $NiCo_2O_4$ loading on the CNFs electrode.

A comparison between the galvanic charge/discharge (GCD) profiles for the three $NiCo_2O_4$:CNFs devices with different loading ratio acquired at a current density of 1A g^{-1} is shown in **Fig. 6 (b).** All the GCD profiles show slightly asymmetric shapes, indicating the quasi-reversible characteristic and nonlinear discharge profile. This behavior is mainly attributed to the integration of the Faradaic characteristic of the $NiCo_2O_4$ nanostructures with the EDL characteristic of the CNFs electrode. Moreover, increasing the loading ratio of the $NiCo_2O_4$ increased the asymmetry of the discharge profiles and also increase the time required to complete one discharge cycle. These results reflect the battery-like behavior of the $NiCo_2O_4$:CNFs devices fabricated from the hybrid electrodes especially those fabricated from the high $NiCo_2O_4$ loadings. In addition to the previous results, the IR drop during the discharging was decreasing with increasing the $NiCo_2O_4$ mass loading. Thus, a preferred interfacial charge transfer is inferred to exist at the $NiCo_2O_4$:CNFs/electrolyte interface.

For the evaluation of the high-capacitive capability of the proposed hybrid electrodes, the specific capacitances C_s of the fabricated SC devices were calculated at different galvanic current densities and plotted in **Fig. 6 (d).** The C_s value calculated at 1 A g^{-1} are and summarized in **Table 2.** The hybrid $NiCo_2O_4$ 2:1 CNFs electrode achieved a superiorly specific capacitance of 540 F g^{-1} at 1 A g^{-1}current density that is higher than 330 F g^{-1} of the $NiCo_2O_4$ 1:1 CNFs device, 250 F g^{-1} of the $NiCo_2O_4$ 1:2 CNFs device, and much higher than 17 F g^{-1} of bare CNFs device. Additionally, the flexible SC device built from the hybrid $NiCo_2O_4$ 2:1 CNFs electrode maintained its superiority at the overall applied GCD current densities and keep showing higher C_s values than the other devices. These significant enhancements in the overall devices' capacitances and performance with increasing the $NiCo_2O_4$ loading on the CNFs electrode are foremost attributed to the unique open structure of nanoflowers and the interconnected nanorods achieved for the high $NiCo_2O_4$ loadings within the hybrid electrodes. However, the observed reduction in *Cs* value with increasing the GCD current is usually attributed in the literature to the decrease in ions adsorption and diffusion rate capability from the electrolyte to the electrode at high charging-discharging rates [39].

Table 2: The electrochemical parameters of all fabricated $NiCo_2O_4$:CNFs and bare CNFs SC devices

SC device	C_s (F g^{-1})	ESR (Ω)	R_{CT} (Ω)	E (Wh Kg^{-1})	P (W Kg^{-1})
CNFs	17	26.9	18.9	13.3	30
$NiCo_2O_4$ 1:2 CNFs	250	26.4	4.6	18.87	227.27
$NiCo_2O_4$ 1:1 CNFs	330	20.8	2.9	22.34	330
$NiCo_2O_4$ 2:1 CNFs	540	17.4	2.7	30	515.38

The electrochemical impedance spectroscopy (EIS) measurement is an effective tool employed here to get an insight assessment on the charge transfer resistances and the

interfacial dynamics of the fabricated devices**. Fig. 6 (e)** displays the EIS Nyquist plots recorded for the $NiCo_2O_4$:CNFs hybrid devices with different loading ratios measured in the frequency range of 10 mHz to 100 kHz. All the fabricated SC devices showed typical Nyquist plots for electrochemical capacitor those consists of a high-frequency small semicircle followed by a straight line in the low-frequency region. The steeper the low-frequency line, the more EDL capacitive nature of a porous electrode. Also, the intercept of the high-frequency small semicircle with the real impedance axis at the high-frequency gives the equivalent series resistance (ESR), whereas its diameter represents the charge transfer resistance (R_{CT}). The source of the R_{CT} of the SC devices is originated from both the EDL effect and Faradic reactions at the hybrid electrode surface.

As seen from **Table 2**, The $NiCo_2O_4$ 2:1 CNFs hybrid electrode showed the lowest ESR ~17.4 Ω, whilst the higher ESR equals 26.4 Ω was obtained from the $NiCo_2O_4$ 1:2 CNFs electrode. This means the $NiCo_2O_4$ 2:1 CNFs possess high intrinsic electric conductivity than the other two electrodes. Furtherly, the very small semicircles were observed for all devices at high-frequency regions, suggesting a fast ion transport and favorable charge transfer across the $NiCo_2O_4$ /electrolyte interface. However, the lowest R_{CT} was obtained for the $NiCo_2O_4$ 2:1 CNFs device. Finally, the steeper low-frequency line of the two devices with high mass loadings of the $NiCo_2O_4$ indicates their higher electrochemical capacitances, in a good agreement with the results from the GCD measurements.

To further clarify the high rate capability and dynamic capacitive behavior of the $NiCo_2O_4$ 2:1 CNFs electrode for standalone SCs application, **Fig. 7(a) and (b)** display the CV voltammograms and GCD profiles measured at different voltage scan rate (5 – 50 mV

s^{-1}) and current densities (1 – 7 A g^{-1}), respectively. Rectangular CV voltammograms were almost recorded for the $NiCo_2O_4$ 2:1 CNFs SC device at the low voltage scan rates (5 and 10 mV s^{-1}) as seen in **Fig. 7 (a).** This referring to the higher contribution of the EDL capacitance effect of the CNFs in the overall capacitive performance of the nanocomposite than the faradic capacitance at the low scan rate. Contrarily, ellipsoidal CV voltammograms were obtained by the device at high voltage scan rates and dominant faradic capacitance contribution can be inferred. This can be explained on the basis of the dynamics of electrolyte ions transportation and redox reactions. Under slow scan rate conditions, and due to the slow ions dynamics, the ions completely penetrate into the pores of the CNFs mat and the EDL capacitance is effectively contributes to the overall capacitance of the device. Conversely, under high voltage scan rate conditions, the electrolyte ions are not having enough time to completely immigrate into the pores of the CNFs mat similar to what likely happened in the case of the slow scan rates. Instead, the faradic electrochemical reactions fastly occurred at the surfaces of the CNFs those completely coated by the $NiCo_2O_4$ nanostructures and nicely wetted with the KOH electrolyte.

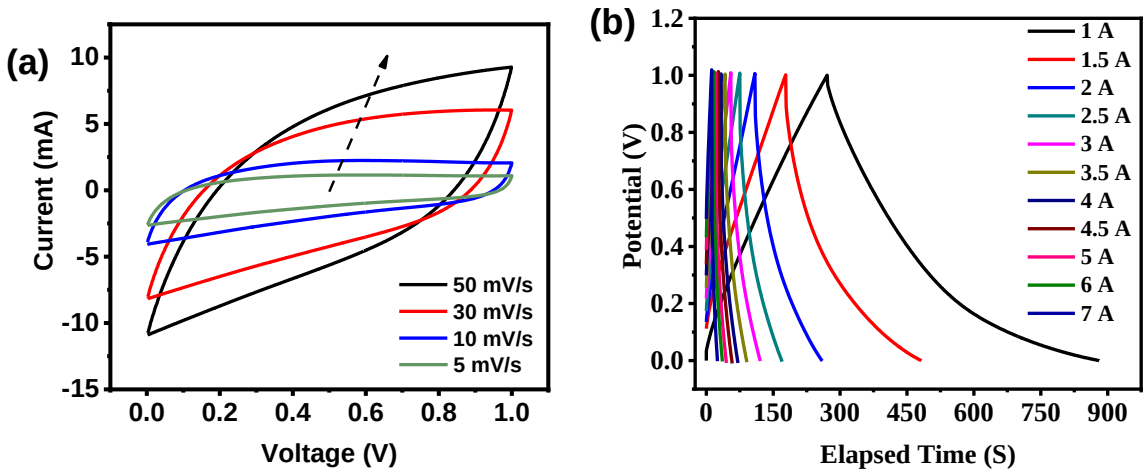

Fig. 7 (a) CV voltammograms at different scan rates, (b) charge-discharge curves at different current densities of the $NiCo_2O_4$ 2:1CNFs two-symmetric electrodes SC device.

The excellent rate capability of the $NiCo_2O_4$ 2:1 CNFs SC device can be seen from the GCD profiles in Fig. 7**(b)**, such that the device was able to complete one charging-discharging cycle at a very high current density of 7 A g^{-1}. This was accompanied by maintaining small IR drops under all tested current densities. Besides, a high coulombic efficiency and high reversibility of the device can be easily noticed from the symmetry between the charging and discharging branches of each recorded GCD profile.

The energy density (*E*, Wh kg^{-1}) the power density (*P*, KW Kg^{-1}) are the two essential factors that must be provided to a clear assess the energy capacity and power delivery capability of any storage device. The *P* and *E* of the SC devices assembled from the $NiCo_2O_4$:CNFs electrode with different loading ratios are calculated using **Equations (3)** and **(4)** and Tabulated in **Table 2**. These *P* and *E* values are schematically presented in Fig. 8 which also compared with the values of SC devices based on NiO:CNFs and Co_3O_4:CNFs hybrid nanocomposites with different mass loadings from the metal oxides. The NiO:CNFs and Co_3O_4:CNFs SC devices are fabricated under the same experimental procedures except using a single metal salt ($Ni(NO_3)_2$ or $Co(NO_3)_2$) in the hydrothermal

reactor instead of using both salts together (see supplementary information **Fig. S1 – S5**). Referring to **Fig. 8** at any given loading ratio, the energy density of the $NiCo_2O_4$:CNFs based device is larger than the obtained values from the NiO:CNFs and Co_3O_4:CNFs SC-based devices and sometimes exceeds devices from higher loadings. A maximum energy density of about 30 Wh kg^{-1} was only obtained from the $NiCo_2O_4$ 2:1 CNFs SC device which is also accompanied by a very high-power delivery of 515.6 W kg^{-1}. However, the comparable power densities of all devices at the same low mass loadings confirm the versatility of our fabricated devices and the ingenuity performance of the CNFs as a standalone electrode.

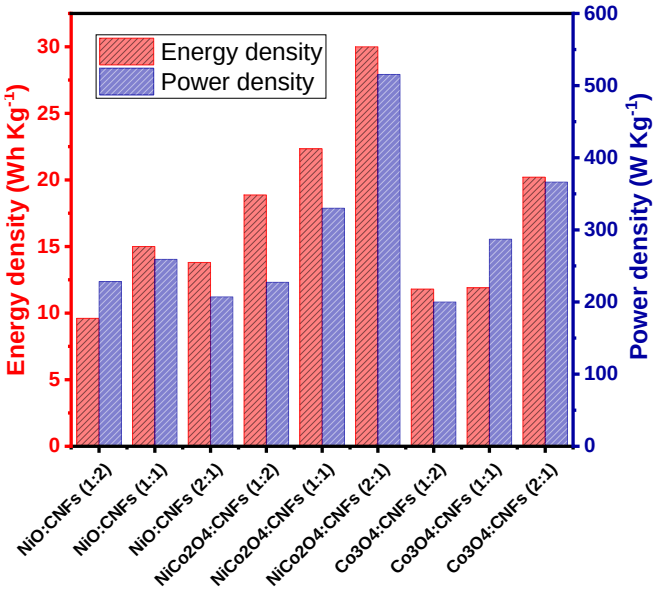

Fig. 8 The energy and power densities of the fabricated two-symmetric electrodes SC devices based on the different metal oxides:CNFs hybrid electrodes.

Finally, the charging and discharging cycle stability for the $NiCo_2O_4$ 2:1 CNFs SC device tested at a current density of 1 A g^{-1} is shown in **Fig. 8**, After 6000 of testing cycles, the $NiCo_2O_4$ 2:1 CNFs SC retained ~ 93.1% of its initial specific capacitance. Such behavior is considered a very satisfactory performance for a prototype electrochemical

storage device assembled with liquid electrolytes and subjected to this large number of charging and discharging cycles at such a slow rate. The assembly with gel electrolyte and using the proper casing are suggested to improve the lifetime and cyclability of the $NiCo_2O_4$:CNFs hybrid SC device but maybe at the expense of the device performance.

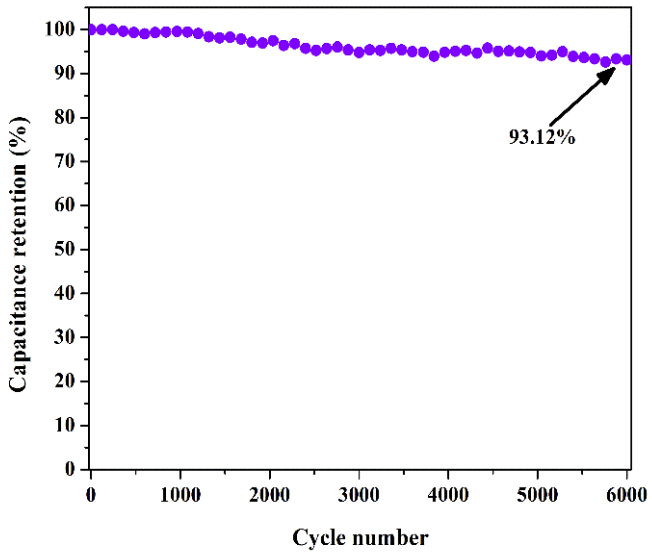

Fig. 9 Galvanic cyclic stability of the NiCo2O4 2:1CNFs two-symmetric electrodes SC device.

4. Conclusions

In summary, we successfully prepared highly-performance $NiCo_2O_4$ and CNFs hybrid electrodes for flexible and substrate-free supercapacitor applications. The facile hydrothermal technique was used to attach spinel $NiCo_2O_4$ nanostructures on the free-standing CNFs electrode of different morphologies and loadings. The CNFs electrode was used as a 3D porous template for the $NiCo_2O_4$ deposition and as well as the current collector of the devices. The best electrochemical performance for the devices is only achievable when the CNFs electrode was loaded with the utmost $NiCo_2O_4$ nanostructure mass loading. The device fabricated by the hybrid electrode that contains twice $NiCo_2O_4$ as much as CNFs

($NiCo_2O_4$ 2:1CNFs) achieved superior electrochemical performance in terms of low charge transfer resistances, higher rate capability, larger specific capacitance, and also longer discharging time. A specific capacitance of 540 F g^{-1} and an energy density of 30 Wh kg^{-1} at a power density of 515.6 W kg^{-1} besides the excellent cycling stability is recoded for the $NiCo_2O_4$ 2:1CNFs supercapacitor. This superior performance of the hybrid nanocomposite is attributed not only to the synergistic integration of EDLC and pseudocapacitive materials together but also to the highly-exposed active surface area, the ultrathin and porous features, shorter ion pathways alongside with the fast electron transport provided by the hierarchical $NiCo_2O_4$ nanostructure tightly anchored on the conductive CNFs electrode.

5. Acknowledgment

The authors gratefully acknowledge the Missions Sector-Higher Education Ministry, Egypt, for the financial support for this work, and the Materials Science and Engineering Department at E-JUST. This study was also supported by Grants (ID 31306) funded by science and technology development fund (STDF) in Egypt.

6. References

[1] K. Jost, D. Stenger, C.R. Perez, J.K. McDonough, K. Lian, Y. Gogotsi, G. Dion, Knitted and screen printed carbon-fiber supercapacitors for applications in wearable electronics, Energy Environ. Sci. 6 (2013) 2698–2705. https://doi.org/10.1039/c3ee40515j.

[2] S.A.N. Tembei, A.M.R.F. El-bab, A. Hessein, A.A. El-moneim, Ultrasonic Doping and Photo-reduction of Graphene Oxide Films for Flexible and High-Performance Electrothermal Heaters, FlatChem. (2020) 100199. https://doi.org/10.1016/j.flatc.2020.100199.

[3] P. Veerakumar, A. Sangili, S. Manavalan, P. Thanasekaran, K.C. Lin, Research Progress on Porous Carbon Supported Metal/Metal Oxide Nanomaterials for Supercapacitor Electrode Applications, Ind. Eng. Chem. Res. 59 (2020) 6347–6374. https://doi.org/10.1021/acs.iecr.9b06010.

[4] S. Zhang, N. Pan, Supercapacitors performance evaluation, Adv. Energy Mater. 5 (2015) 1–19. https://doi.org/10.1002/aenm.201401401.

[5] T. Chen, L. Dai, Flexible supercapacitors based on carbon nanomaterials, J. Mater. Chem. A. 2 (2014) 10756–10775. https://doi.org/10.1039/c4ta00567h.

[6] Y. Qiu, G. Li, Y. Hou, Z. Pan, H. Li, W. Li, M. Liu, F. Ye, X. Yang, Y. Zhang, Vertically aligned carbon nanotubes on carbon nanofibers: A hierarchical three-dimensional carbon nanostructure for high-energy flexible supercapacitors, Chem. Mater. 27 (2015) 1194–1200. https://doi.org/10.1021/cm503784x.

[7] D. Ma, J. Cai, X. Wu, H. Xu, Y. Tian, H. Zhao, Treatment of multiwall carbon nanotubes based on the modified Hummers method for supercapacitor electrode materials, J. Renew. Sustain. Energy. 8 (2016). https://doi.org/10.1063/1.4941856.

[8] E. Ghoniem, S. Mori, A. Abdel-Moniem, Low-cost flexible supercapacitors based on laser reduced graphene oxide supported on polyethylene terephthalate substrate, J. Power Sources. 324 (2016) 272–281. https://doi.org/10.1016/j.jpowsour.2016.05.069.

[9] A. Abd El-Moneim, A. E. Rashed, Two steps synthesis approach of MnO2/graphene nanoplates/graphite composite electrode for supercapacitor application, Mater. Today Energy. 3 (2017) 24–31. https://doi.org/10.1016/j.mtener.2017.02.004.

[10] B. Liu, L. Liu, Y. Yu, Y. Zhang, A. Chen, Synthesis of mesoporous carbon with tunable pore size for supercapacitors, New J. Chem. 44 (2020) 1036–1044. https://doi.org/10.1039/c9nj05085j.

[11] M.H. El-Shafei, E. Ghoniem, A.H. Hassanin, A.A. El-Moneim, Novel technique for producing porous carbon nanofiber mate for supercapacitors application, 2017. https://doi.org/10.4028/www.scientific.net/KEM.735.199.

[12] Z. Wu, Y. Zhu, X. Ji, NiCo2O4-based materials for electrochemical supercapacitors, J. Mater. Chem. A. 2 (2014) 14759–14772. https://doi.org/10.1039/c4ta02390k.

[13] H. Ma, Z. Liu, X. Wang, C. Zhang, R. Jiang, Supercapacitive performance of porous carbon materials derived from tree leaves, J. Renew. Sustain. Energy. 9 (2017). https://doi.org/10.1063/1.4997019.

[14] J. Ma, Q. Guo, H.L. Gao, X. Qin, Synthesis of C60/Graphene composite as electrode in supercapacitors, Fullerenes Nanotub. Carbon Nanostructures. 23 (2015) 477–482. https://doi.org/10.1080/1536383X.2013.865604.

[15] S. Vijayakumar, S. Nagamuthu, G. Muralidharan, Supercapacitor studies on NiO nanoflakes synthesized through a microwave route, ACS Appl. Mater. Interfaces. 5 (2013) 2188–2196. https://doi.org/10.1021/am400012h.

[16] D. Majumdar, T. Maiyalagan, Z. Jiang, Recent Progress in Ruthenium Oxide-Based Composites for Supercapacitor Applications, ChemElectroChem. 6 (2019) 4343–4372. https://doi.org/10.1002/celc.201900668.

[17] M. Huang, F. Li, F. Dong, Y.X. Zhang, L.L. Zhang, MnO2-based nanostructures for high-performance supercapacitors, J. Mater. Chem. A. 3 (2015) 21380–21423. https://doi.org/10.1039/c5ta05523g.

[18] C. Rong, S. Chen, J. Han, K. Zhang, D. Wang, X. Mi, X. Wei, Hybrid supercapacitors integrated rice husk based activated carbon with LiMn2O4, J. Renew. Sustain. Energy. 7 (2015). https://doi.org/10.1063/1.4913965.

[19] L. Li, Z.Y. Qin, L.F. Wang, H.J. Liu, M.F. Zhu, Anchoring alpha-manganese oxide nanocrystallites on multi-walled carbon nanotubes as electrode materials for supercapacitor, J. Nanoparticle Res. 12 (2010) 2349–2353. https://doi.org/10.1007/s11051-010-9980-8.

[20] B. Ren, M. Fan, Q. Liu, J. Wang, D. Song, X. Bai, Hollow NiO nanofibers modified by citric acid and the performances as supercapacitor electrode, Electrochim. Acta. 92 (2013) 197–204. https://doi.org/10.1016/j.electacta.2013.01.009.

[21] F. Manteghi, S.H. Kazemi, M. Peyvandipour, A. Asghari, Preparation and application of cobalt oxide nanostructures as electrode materials for electrochemical supercapacitors, RSC Adv. 5 (2015) 76458–76463. https://doi.org/10.1039/c5ra09060a.

[22] L. Gao, S. Xu, C. Xue, Z. Hai, D. Sun, Y. Lu, Self-assembly of hierarchical 3D starfish-like Co3O4 nanowire bundles on nickel foam for high-performance supercapacitor, J. Nanoparticle Res. 18 (2016) 1–10. https://doi.org/10.1007/s11051-016-3419-9.

[23] B.J. Lee, S.R. Sivakkumar, J.M. Ko, J.H. Kim, S.M. Jo, D.Y. Kim, Carbon nanofibre/hydrous RuO2 nanocomposite electrodes for supercapacitors, J. Power Sources. 168 (2007) 546–552. https://doi.org/http://dx.doi.org/10.1016/j.jpowsour.2007.02.076.

[24] a. a. El-Moneim, E. Akiyama, K.M. Ismail, K. Hashimoto, Corrosion behaviour of sputter-deposited Mg-Zr alloys in a borate buffer solution, Corros. Sci. 53 (2011) 2988–2993. https://doi.org/10.1016/j.corsci.2011.05.043.

[25] K.M. El-Khatib, M.O. Abou Helal, A.A. El-Moneim, H. Tawfik, Corrosion stability of SUS316L HVOF sprayed coatings as lightweight bipolar plate materials in PEM fuel cells, Anti-Corrosion Methods Mater. 51 (2004) 136–142. https://doi.org/10.1108/00035590410523238.

[26] M. Gamil, O. Tabata, K. Nakamura, A.M.R.F. El-Bab, A.A. El-Moneim, Investigation of a new high sensitive micro-electromechanical strain gauge sensor based on graphene piezoresistivity, Key Eng. Mater. 605 (2014) 207–210. https://doi.org/10.4028/www.scientific.net/KEM.605.207.

[27] L. Yang, S. Cheng, Y. Ding, X. Zhu, Z.L. Wang, M. Liu, Hierarchical network architectures of carbon fiber paper supported cobalt oxide nanonet for high-capacity pseudocapacitors, Nano Lett. 12 (2012) 321–325. https://doi.org/10.1021/nl203600x.

[28] S. Jeon, J.H. Jeong, H. Yoo, H.K. Yu, B.H. Kim, M.H. Kim, RuO2 Nanorods on Electrospun Carbon Nanofibers for Supercapacitors, ACS Appl. Nano Mater. 3 (2020) 3847–3858. https://doi.org/10.1021/acsanm.0c00579.

[29] W. Luo, H. Xue, The synthesis and electrochemical performance of NiCo 2 O 4 embedded carbon nanofibers for high-performance supercapacitors, Fullerenes Nanotub. Carbon Nanostructures. 27 (2019) 189–197. https://doi.org/10.1080/1536383X.2018.1538131.

[30] J. Du, G. Zhou, H. Zhang, C. Cheng, J. Ma, W. Wei, L. Chen, T. Wang, Ultrathin porous NiCo2O4 nanosheet arrays on flexible carbon fabric for high-performance supercapacitors, ACS Appl. Mater. Interfaces. 5 (2013) 7405–7409. https://doi.org/10.1021/am4017335.

[31] F. Deng, L. Yu, G. Cheng, T. Lin, M. Sun, F. Ye, Y. Li, Synthesis of ultrathin mesoporous NiCo2O4 nanosheets on carbon fiber paper as integrated high-performance electrodes for supercapacitors, J. Power Sources. 251 (2014) 202–207. https://doi.org/10.1016/j.jpowsour.2013.11.048.

[32] M.H. El-Shafei, A. Hassanin, N. Shaalan, T. Sharshar, A. Abdelmoneim, Free-standing interconnected carbon nanofibers electrodes: new structural designs for supercapacitor application., Nanotechnology. (2020). https://doi.org/10.1088/1361-6528/ab6d22.

[33] A.G. El-Deen, A.G. El-Deen, M. Hussein El-Shafei, M. Hussein El-Shafei, A. Hessein, A. Hessein, A.H. Hassanin, N.M. Shaalan, N.M. Shaalan, A.A. El-Moneim, A.A. El-Moneim, A.A. El-Moneim, High-performance asymmetric

supercapacitor based hierarchical NiCo2O4@ carbon nanofibers//Activated multichannel carbon nanofibers, Nanotechnology. 31 (2020). https://doi.org/10.1088/1361-6528/ab97d6.

[34] Y. Xu, L. Wang, P. Cao, C. Cai, Y. Fu, X. Ma, Mesoporous composite nickel cobalt oxide/graphene oxide synthesized via a template-assistant co-precipitation route as electrode material for supercapacitors, J. Power Sources. 306 (2016) 742–752. https://doi.org/10.1016/j.jpowsour.2015.12.106.

[35] M. Adel, R. Abdel-Karim, A. Abdelmoneim, Studying the conversion of graphite into nanographene sheets using supercritical phase exfoliation method, Fullerenes Nanotub. Carbon Nanostructures. 28 (2020) 589–602. https://doi.org/10.1080/1536383X.2020.1725747.

[36] J. Hu, M. Li, F. Lv, M. Yang, P. Tao, Y. Tang, H. Liu, Z. Lu, Heterogeneous NiCo2O4@polypyrrole core/sheath nanowire arrays on Ni foam for high performance supercapacitors, J. Power Sources. 294 (2015) 120–127. https://doi.org/10.1016/j.jpowsour.2015.06.049.

[37] G. Zhang, X.W.D. Lou, Controlled growth of NiCo2 O4 nanorods and ultrathin nanosheets on carbon nanofibers for high-performance supercapacitors, Sci. Rep. 3 (2013) 2–7. https://doi.org/10.1038/srep01470.

[38] J. Shen, X. Li, N. Li, M. Ye, Facile synthesis of NiCo2O4-reduced graphene oxide nanocomposites with improved electrochemical properties, Electrochim. Acta. 141 (2014) 126–133. https://doi.org/10.1016/j.electacta.2014.07.063.

[39] N. Choudhary, C. Li, J. Moore, N. Nagaiah, L. Zhai, Y. Jung, J. Thomas, Asymmetric Supercapacitor Electrodes and Devices, Adv. Mater. 29 (2017). https://doi.org/10.1002/adma.201605336.